Use of Absorption Cross Section to Predict Coherence Bandwidth and Other Characteristics of a Reverberation Chamber Setup for Wireless-System Tests

Jos N. H. Dortmans, *Student Member, IEEE*, Kate A. Remley, *Fellow, IEEE*, Damir Senić, *Member, IEEE*, Chih-Ming Wang, and Christopher L. Holloway, *Fellow, IEEE*

Abstract—**We present a method to predict the coherence bandwidth, delay spread, and power transfer function of a reverberation chamber. With an *S*-parameter measurement of an unloaded chamber and a measurement of one loading condition, the characteristics for other loading conditions can be predicted. The method is based on the absorption cross section of the absorbing material that is added to the chamber. We tested this method in two different reverberation chambers and for different types, shapes, and orientations of absorbing material. For all evaluated cases, the differences between the predicted and measured characteristics were below 6.2%.**

Index Terms—**Absorption cross section, coherence bandwidth, delay spread, over-the-air (OTA) test, power transfer function, reverberation chamber (RC), wireless system.**

I. INTRODUCTION

REVERBERATIONS chambers (RCs) are becoming popular for testing the performance of wireless devices and can be used to simulate different multipath environments [1]–[10]. RCs are very popular measurement environments in the wireless community due to their adaptive nature. By loading the RC with different amounts of RF absorber we can replicate various real-world environments.

The coherence bandwidth (CBW) and the root-mean-square (RMS) delay spread τ_{RMS} are important characteristics of the RC and are related to each other by an inverse relationship [2], [3], [6]. The CBW is the bandwidth over which the frequencies are correlated. If a signal has a bandwidth narrower than the CBW, the channel is expected to be frequency flat. If the signal bandwidth is higher than the CBW, the channel is frequency selective and this may cause errors in demodulation of the received signal [2], [3], [5], [9]. By a channel, we mean the medium used to transmit a signal [11]. The CBW of the RC

needs to be wider than the signal bandwidth of the device under test (DUT). The time-domain equivalent of a narrow CBW is a long τ_{RMS} resulting in intersymbol interference.

The CBW and τ_{RMS} of the RC can be changed by adding RF absorbing material to the chamber. Adding RF absorber will lower the Q factor [4], [8], [10], widen the CBW [3], [10], [12], and shorten τ_{RMS} [2], [4]. Loading the RC reduces the spatial uniformity and increases the measurement uncertainties [7], [8], [10], [12].

For power-related DUT measurements such as total radiated power and total isotropic sensitivity (TIS), the chamber reference power transfer function G_{ref} is an important quantity. G_{ref} is similar to the range path loss of an anechoic chamber [10]. For calculations of the actual sent or received power by the DUT, the path loss in the RC is needed.

In past research work [10], RCs were iteratively loaded with RF absorbers. For every loading case, the CBW was calculated from measured *S*-parameters. If the CBW was too narrow, a piece of absorber was added and the CBW was measured again. This process was repeated until the desired CBW was reached. These measurements were time consuming. Time can be saved by predicting the CBW for a given amount of RF absorber with known properties and for known properties of the unloaded RC.

Previous research work [13] focused on predicting the CBW from the dimensions of the absorbing surface and from the permittivity of the absorbing material. From the absorption cross section (ACS) of the absorbers, the change in CBW versus the number of absorbers was estimated. Amador *et al.* [14] used the ACS of one object to deduce the effect of N absorbing objects on the Q factor and time response of the RC. For this prediction, a three-dimensional model of the absorber was needed.

This paper will focus on the prediction of the CBW, τ_{RMS}, and G_{ref} without knowing the electrical parameters of the RF absorber in advance. We have developed a method to predict these metrics of the RC setup with a measurement of the unloaded chamber and a measurement of a single loading case. We will consider different types of absorbing material and different setups to evaluate the method.

The systematic overview of the paper is as follows: Section II describes theoretical background needed for the prediction of RC characteristics. We use ACS as a metric to predict the chamber characteristic, so we relate ACS to CBW, τ_{RMS}, and G_{ref} in this section. In Section III, we describe the setups

we measured and procedures we used to acquire data needed to show the prediction method. Section IV is divided in three parts. The first part shows the influence of the vector network analyzer (VNA) setup on the resulting chamber characteristics. The second part gives the results of the chamber characteristics predicted from multiple loading measurements. The last part uses the results of the second part to predict chamber characteristics from a single loading measurement. We draw conclusion in Section V.

II. THEORY

The ACS provides the effective absorbing quality of an absorbing object and is an important metric of lossy objects. The ACS of different objects was studied in [15] and [16]. The ACS in m^2 of an absorbing object can be determined from its contribution to the Q factor of the RC, as discussed in [17, Sec. 10.4]

$$\langle ACS \rangle_{N,M,f} = \frac{2\pi V}{\lambda} Q_{abs}^{-1} \quad (m^2). \quad (1)$$

In (1), V is the volume of the RC in m^3, λ is the free space wavelength in m, and Q_{abs} is the Q factor contribution of the absorbing object. The chevrons denote the average over the paddle stirring positions N, antenna stirring positions M, and frequency points f. The inverse Q factor of the loaded RC can be written as the Q factor of the unloaded RC added in inverse with the Q factor contribution of the absorbing object

$$Q_L^{-1} = Q_U^{-1} + Q_{abs}^{-1}. \quad (2)$$

By combining (1) and (2), we can write the ACS as a function of the Q factor of the loaded and unloaded RC

$$\langle ACS \rangle_{N,M,f} = \frac{2\pi V}{\lambda} \left(Q_L^{-1} - Q_U^{-1} \right) \quad (m^2). \quad (3)$$

We can relate τ_{RMS} to Q by [4], [6], [17]

$$Q_L = \omega \langle \tau_{RMS}^L \rangle_{N,M,f} \quad \text{and} \quad Q_U = \omega \langle \tau_{RMS}^U \rangle_{N,M,f}, \quad (4)$$

where $\langle \tau_{RMS}^L \rangle_{N,M,f}$ and $\langle \tau_{RMS}^U \rangle_{N,M,f}$ are the chamber time constants for the loaded and unloaded RC, respectively. We found τ_{RMS} from the square root of the second-central moment of the power delay profile (PDP), described in [4]. Values of the PDP reaching the noise floor were removed. We also calculated τ_{RMS} using different methods. τ_{RMS} determined by removing early time response and from an exponential fit to the PDP gave similar results. By combining (3) and (4) and using $\omega = 2\pi c/\lambda$, we can write the ACS as a function of the time constant of the loaded and unloaded RC

$$\langle ACS \rangle_{N,M,f} = \frac{V}{c} \left(\frac{1}{\langle \tau_{RMS}^L \rangle_{N,M,f}} - \frac{1}{\langle \tau_{RMS}^U \rangle_{N,M,f}} \right) \quad (m^2), \quad (5)$$

where c is the speed of light in free space in m/s. If we change the order of the variables in (5), we can calculate τ_{RMS}^L as an inverse function of ACS and τ_{RMS}^U

$$\langle \tau_{RMS}^L \rangle_{N,M,f} = \left(\frac{\langle ACS \rangle_{N,M,f} \cdot c}{V} + \frac{1}{\langle \tau_{RMS}^U \rangle_{N,M,f}} \right)^{-1} \quad (s). \quad (6)$$

Using (6), we can predict τ_{RMS}^L if we know τ_{RMS}^U and the ACS of an absorbing object placed in the RC. τ_{RMS}^U can be determined by calculating the PDP from S-parameters, described in [4] and [6].

Equations (1) and (6) were derived for an RC with good spatial uniformity. This paper empirically shows that these relationships hold even for heavily loaded RCs. Now we replace τ_{RMS} in (5) with CBW for both the loaded and unloaded chamber, where τ_{RMS} can be calculated from CBW following [2], [3], [6]

$$\tau_{RMS} = \frac{\sqrt{3}}{CBW\pi} \quad (s), \quad (7)$$

which was originally calculated for an ideal RC. The CBW can be determined from S-parameters applying an autocorrelation function [5]

$$R(\Delta f, n) = \int_{-\infty}^{\infty} S_{21}(f,n) S_{21}^*(f + \Delta f, n) df. \quad (8)$$

The CBW is defined as the frequency band for which the autocorrelation lies above a certain threshold. A higher threshold results in a flatter channel. The choice of the threshold depends on the receiver to be tested [18]. In this study, we use a threshold of 0.5 because the devices we intend to test have error correction.

By combining (5) and (7), we obtain the ACS as a function of the CBW of the loaded and unloaded RC

$$\langle ACS \rangle_{N,M,f} = \frac{V\pi}{\sqrt{3}c} \left(CBW^L - CBW^U \right) \quad (m^2). \quad (9)$$

Rearranging (9), we can calculate CBW^L as a function of the ACS and CBW^U

$$CBW^L = \frac{\langle ACS \rangle_{N,M,f} \sqrt{3}c}{V\pi} + CBW^U \quad (Hz). \quad (10)$$

With (10), CBW^L can be predicted from the ACS of the RF absorber and CBW^U.

From [19] and [20], it follows that the ACS can also be calculated from the G_{ref} of the RC. The Q factor of the unloaded and loaded RC can be written as [17]

$$Q_U = \frac{16\pi^2 V}{\lambda^3} \frac{\langle P_{rU} \rangle_{N,M,f}}{P_t} \quad \text{and} \quad Q_L = \frac{16\pi^2 V}{\lambda^3} \frac{\langle P_{rL} \rangle_{N,M,f}}{P_t}, \quad (11)$$

where P_t is the transmitted power, $\langle P_{rU} \rangle_{N,M,f}$ is the average received power of the unloaded RC, and $\langle P_{rL} \rangle_{N,M,f}$ is the average received power of the loaded RC. Following [17, eq. 10.28], we can combine (3) and (11), giving the ACS as

$$\langle ACS \rangle_{N,M,f} = \frac{\lambda^2 P_t}{8\pi} \left(\frac{1}{\langle P_{rL} \rangle_{N,M,f}} - \frac{1}{\langle P_{rU} \rangle_{N,M,f}} \right) \quad (m^2). \quad (12)$$

Characterization of an RC is often carried out with a VNA that measures S-parameters. For perfectly matched antennas, a measurement of the forward transmission coefficient S_{21} is sufficient. The square of S_{21} is equal to the ratio of the received power and the transmitted power. However, the antennas are not perfectly matched which causes reflections at the antenna ports.

We can correct the reflections by using the transfer function G

$$G = \frac{\langle |S_{21}|^2 \rangle_{N,M,f}}{\left(1 - |\langle S_{11} \rangle_{N,M,f}|^2\right)\left(1 - |\langle S_{22} \rangle_{N,M,f}|^2\right)}, \quad (13)$$

where S_{11} is the reflection coefficient of the transmit antenna and S_{22} is the reflection coefficient of the receive antenna.

Also, the efficiencies of the transmit and receive antennas are not perfect. By correcting (13) with the transmit antenna radiation efficiency e_t and the receive antenna radiation efficiency e_r, we get

$$G_{\text{ref}} = \frac{\langle |S_{21}|^2 \rangle_{N,M,f}}{\left(1 - |\langle S_{11} \rangle_{N,M,f}|^2\right)\left(1 - |\langle S_{22} \rangle_{N,M,f}|^2\right) e_t e_r}. \quad (14)$$

For the DUT measurements, we correct only for the efficiency of the transmit antenna because the receive antenna will be the same in VNA and DUT measurements and e_r will cancel out [10]. Using (12) and (14), we get

$$\langle \text{ACS} \rangle_{N,M,f} = \frac{\lambda^2}{8\pi}\left(\frac{1}{G_{\text{ref}}^L} - \frac{1}{G_{\text{ref}}^U}\right) \quad (\text{m}^2). \quad (15)$$

By rearranging (15), we can calculate G_{ref}^L as an inverse function of the ACS and G_{ref}^U

$$G_{\text{ref}}^L = \left(\frac{\langle \text{ACS} \rangle_{N,M,f} \cdot 8\pi}{\lambda^2} + \frac{1}{G_{\text{ref}}^U}\right)^{-1}. \quad (16)$$

In (16), G_{ref}^L can be predicted if we know the ACS of the RF absorber and G_{ref}^U. We can calculate G_{ref}^U from S-parameters and by knowing the efficiencies of the transmit and receive antennas with (14).

In the following sections, we evaluate the predictive ability of (6), (10), and (16) for a number of RC setups.

III. MEASUREMENT SETUP

The measurements were made inside two different RCs located at the National Institute of Standards and Technology, Boulder, CO, USA. The dimensions of the large RC are 4.6 m (l) × 3.1 m (w) × 2.8 m (h). The RC contains one mechanical metal mode stirrer tracing out a cylinder with radius 0.5 m and height 2.1 m mounted between the floor and ceiling of the chamber. The dimensions of the small RC are 1.5 m (l) × 1.2 m (w) × 1.5 m (h), and it contains a single mechanical metal mode stirrer tracing out a cylinder with radius 0.3 m and height 1.1 m mounted between the floor and ceiling of the chamber.

For both RCs, a double-ridged horn antenna (DRHA) and a discone antenna were placed inside (see Fig. 1). The DRHA was pointed away from the omnidirectional discone antenna so no large line-of-sight component was created. The DRHA and the discone antenna had operating frequency ranges of 1 GHz–18 GHz and 0.65 GHz–3.5 GHz, respectively. The discone antenna was connected to port 1 of a VNA and served as the transmit antenna. The DRHA was connected to port 2 of the VNA and served as the receive antenna. The antennas were placed at least a half wavelength away from the walls and metal objects and at an enough distance away from absorbing materials to prevent
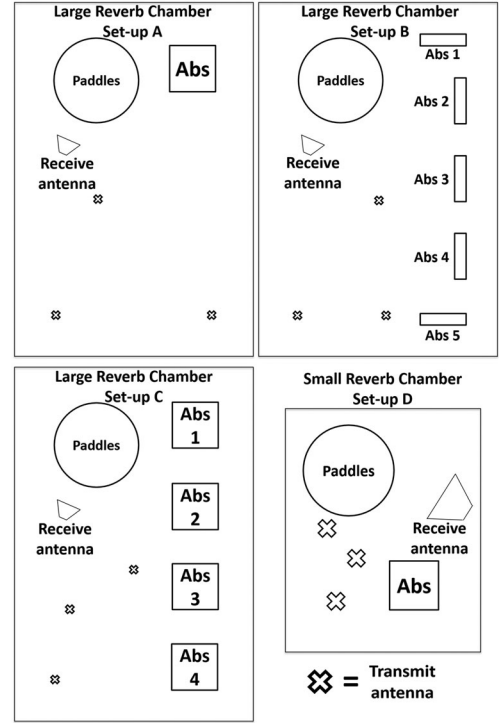

Fig. 1. RC measurement setups. Top row from left to right: Setup A and Setup B. Bottom row from left to right: Setup C and Setup D. The large Xs indicate the locations of the transmit antenna for each measurement. Setups are defined in Table I.

the proximity effect [18]. The positions of the receive antenna were chosen such that there is no spatial correlation between them. S-parameters were measured from 800 MHz to 900 MHz (cell band) and 1850 MHz to 2000 MHz (personal communications service (PCS) band) with a frequency spacing of 50 kHz; hence, 2001 and 3001 points were measured in these frequency bands, respectively. For the small RC, we only measured the PCS band because based on our previous measurements, the lowest usable frequency for this RC is approximately 900 MHz. For all setups, S-parameters were collected for 72 stepped positions of the mechanical stirrer with 5° spacing, so one complete revolution of the stirrer was measured.

We used four setups with different types, shapes, and placement of absorbers inside the two different RCs. Fig. 2 shows a photograph of Setup A loaded with seven RF absorber blocks. As described in Table I, we used two different sets of layered RF absorber blocks of size 0.61 m × 0.61 m × 0.15 m in two different loading configurations. The overall exposed surface area of a configuration is a reasonable metric to use for predicting ACS and other characteristics [21]. We also used one set of small RF absorbers blocks with size 0.30 m × 0.30 m × 0.15 m and one set of pyramidal absorbers. The size of the base of the pyramidal absorber was 0.60 m × 0.60 m × 0.10 m and contained 3 × 3 pyramids with height 0.49 m and a base of 0.20 m × 0.20 m. The total exposed surface of one pyramidal absorber was 2.0 m² (the bottom of the absorber is not visible because it lies on the metal floor). Table I summarizes the measurement setups.

Fig. 2. Picture of Setup A. The antenna in the left back of the RC is the receive antenna and in the left front is the transmit antenna. The mechanical stirrer is located in the left back of the chamber and the absorbers are placed in the right back of the chamber.

TABLE I
SUMMARY OF MEASUREMENT SETUPS

	Setup A	Setup B	Setup C	Setup D
RC	Large RC	Large RC	Large RC	Small RC
Absorber type	Block set 1	Block set 2	Pyramidal	Small block
Number of absorbers	1 to 7	1 to 5	1 to 4	1 to 5
Absorber placement	In a stack	On the side	On the floor	In a stack
Antenna positions	3	3	3	3
Antenna orientations per position	3	1	1	1
Exposed surface 1 absorber	0.74 m^2	1.0 m^2	2.0 m^2	0.27 m^2

Exposed surface area of one absorber placed in the RC. Adding absorber in a stack will not add the same amount of surface area.

TABLE II
RELATIONSHIP BETWEEN NUMBER OF POINTS PER MHZ AND FREQUENCY SPACING

Frequency points per MHz	Frequency spacing Δf (kHz)
0.5	2000
1	1000
2	500
2.5	400
5	200
10	100
20	50

IV. MEASUREMENT RESULTS

A. VNA Setup for CBW, τ_{RMS}, and G_{ref} Measurements

The ACS can be calculated from τ_{RMS} with (5), from G_{ref} with (15), or from CBW with (9). However, we must ensure that these values are computed from a sufficient number of frequency points for a given RC setup in order to obtain a reliable result. We calculated τ_{RMS}, G_{ref}, and CBW for Setup A using different numbers of frequency points per MHz by decimating the collected data, as shown in Table II.

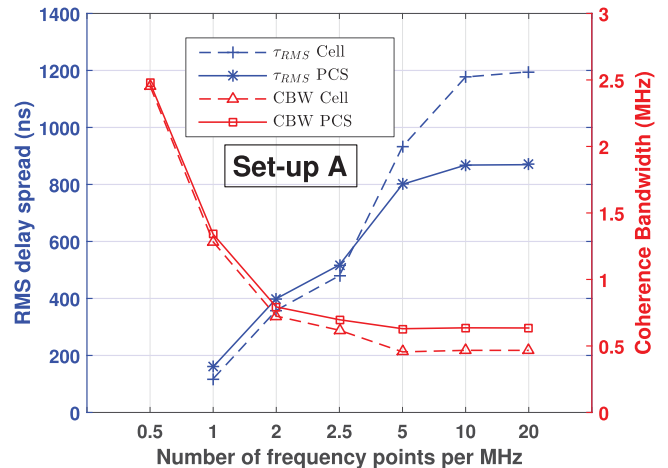Fig. 3. τ_{RMS} and CBW as a function of the number of measured frequency points for the unloaded large RC (Setup A) calculated for the cell and PCS bands.
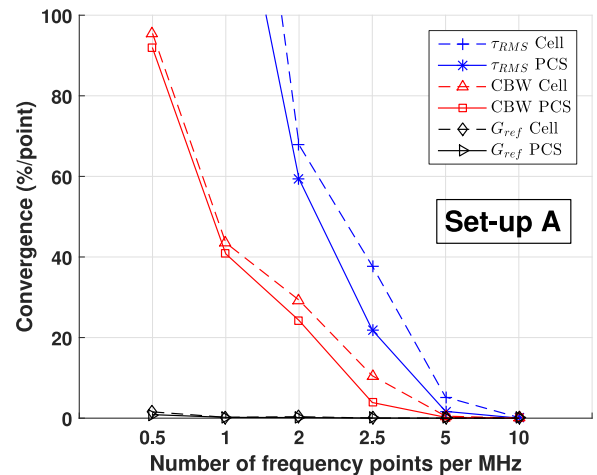

Fig. 4. Convergence of τ_{RMS}, G_{ref}, and CBW for the unloaded large RC (Setup A). The graph shows the percent difference between the current point and the next point calculated for the cell and PCS bands.

Fig. 3 shows τ_{RMS} and CBW for different numbers of frequency points. Fig. 4 shows the convergence of τ_{RMS}, CBW, and G_{ref}. By convergence, we mean the percent difference between two consecutive points. We say that a value is converged when the convergence is less than 5% per frequency point. The calculations for these figures were made for the cell and PCS bands. We show measurements made in an unloaded RC, because in an unloaded RC, the convergence is slowest. The CBW converges faster than τ_{RMS}, to within 5%, at 5 points per MHz for this RC setup. For the calculation of G_{ref}, the number of points needed is not large and G_{ref} has already converged at 0.5 points per MHz.

We also studied the number of frequency points needed for the calculation of τ_{RMS}, G_{ref}, and CBW for the small RC (Setup D). Fig. 5 shows the convergence with increasing number of frequency points per MHz for the unloaded small RC for the PCS band. For this RC setup, the CBW again converges faster
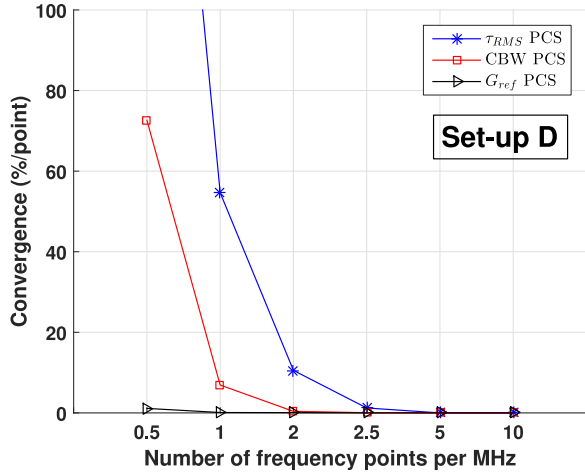
Fig. 5. Convergence of τ_{RMS}, G_{ref}, and CBW for the unloaded small RC (Setup D). The graph shows the percent difference between the current point and the next point calculated for the PCS band.
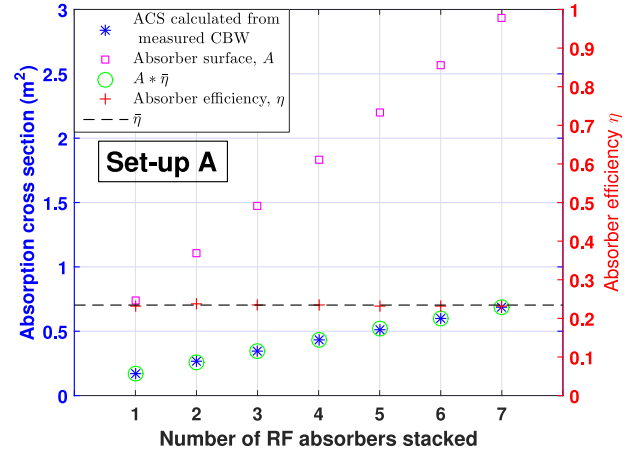

Fig. 6. ACS calculated for the PCS band from (9) (stars), exposed absorber surface area (squares), η (plusses), and exposed absorber surface area times $\bar{\eta}$ (0.23) for different loadings of the RC (circles).

TABLE III
$\bar{\eta}$ AND MAXIMUM DIFFERENCE BETWEEN MEASURED AND PREDICTED CBW, τ_{RMS}, AND G_{REF} PREDICTED FROM MULTIPLE LOADING CONDITIONS

Setup	$\bar{\eta}_{\text{CBW}}$	$\Delta_{\max}$ CBW (%)	$\bar{\eta}_{\tau_{\text{RMS}}}$	$\Delta_{\max}$ τ_{RMS} (%)	$\bar{\eta}_{G_{\text{ref}}}$	$\Delta_{\max}$ G_{ref} (dB)
A Cell	0.25	1.9	0.24	2.9	0.25	0.067
A *PCS*	*0.23*	*1.2*	*0.23*	*3.2*	*0.25*	*0.057*
B Cell	0.21	1.9	0.20	2.8	–	–
B *PCS*	*0.20*	*3.2*	*0.20*	*2.4*	*–*	*–*
C Cell	0.15	3.1	0.15	2.3	–	–
C *PCS*	*0.15*	*1.7*	*0.14*	*2.2*	*–*	*–*
D *PCS*	*0.24*	*3.2*	*0.23*	*3.0*	*–*	*–*

than the τ_{RMS} and the G_{ref} has again converged at 0.5 points per MHz. The CBW has converged to within 5% at two frequency points per MHz.

We see that the number of frequency points needed for the calculation of τ_{RMS} and CBW depends on the RC. Also, the CBW is dependent on the RC. For the PCS band, CBW$^{\text{U}}$ of the large RC is about 0.5 MHz and CBW$^{\text{U}}$ of the small RC is about 1.7 MHz. So, for an RC with a smaller CBW, a smaller frequency spacing is needed than for an RC with a larger CBW. The difference in CBW between the two RCs can be explained by the Q factor. From (11), the Q factor is proportional to the volume of the RC, so a larger RC has a larger Q factor. Equation (4) shows that the Q factor is proportional to τ_{RMS}, and from (7) τ_{RMS} is inversely proportional to CBW. Hence, the large RC has a lower CBW than the small RC.

B. Predicting CBW, $\tau_{\mathbf{RMS}}$, and $G_{\mathbf{ref}}$ From Multiple Loading Conditions

In this section, we focus on calculating the ACS with the CBW using (9) and predicting the CBW from (10). The results for τ_{RMS} and G_{ref} can be found in Table III. For G_{ref} we only use Setup A because for G_{ref} measurements, nine antenna positions are needed for results to converge [7].

Fig. 6 shows the ACS as a function of the number of absorbers stacked in the large RC (Setup A) for the PCS band. The squares show the actual exposed surface area of the absorbers. The stars show the ACS calculated from (9). If the absorbers were ideal, the calculated ACS would be equal to the actual exposed surface area divided by four [22], [23]. The plus markers show the ratio of the ACS to the exposed absorber surface area. We define this ratio as a correction factor η that accounts for the limited efficiency of the RF absorber

$$\eta = \frac{\langle \text{ACS} \rangle}{A} \stackrel{\text{ideal}}{=} \frac{A/4}{A} = 0.25 \qquad (17)$$

where A is the exposed surface area of the absorber. ACS and A have the same units. The circles show the exposed surface area of the absorbers times the mean of η, where η was calculated for each loading case. From Fig. 6, we see that η is approximately constant (the maximum difference in η is 0.66%). We define $\bar{\eta}$ as the average of η for all loading conditions. Multiplying $\bar{\eta}$ with the actual exposed surface area of the absorbers agrees to within 2% of the calculated ACS. Therefore, we conclude that the ACS is a linear function of the exposed surface area of the absorber.

We can predict the CBW of the RC setup for other loading cases from (10) by knowing CBW$^{\text{U}}$, the speed of light, the volume of the RC, and the ACS of the new load. In Fig. 7, the predicted CBW and the CBW obtained from (8) for various loading conditions are compared for the PCS band. Measurements were conducted at multiple transmit antenna locations to account for the reduction in spatial uniformity with loading [10], [12] as shown in Table I. The stars show the measured CBW [calculated from (8)]. The squares show the CBW calculated from (10) with the actual exposed surface area of the absorbers as ACS. A discussion of the effects of exposing various amounts of surface area may be found in [24]. There is a significant difference between the measured and calculated CBW when we use the actual exposed surface area as ACS. The circles show the CBW calculated from (10) for the actual exposed surface area of the absorbers multiplied by the $\bar{\eta}$ from Fig. 6, as ACS.
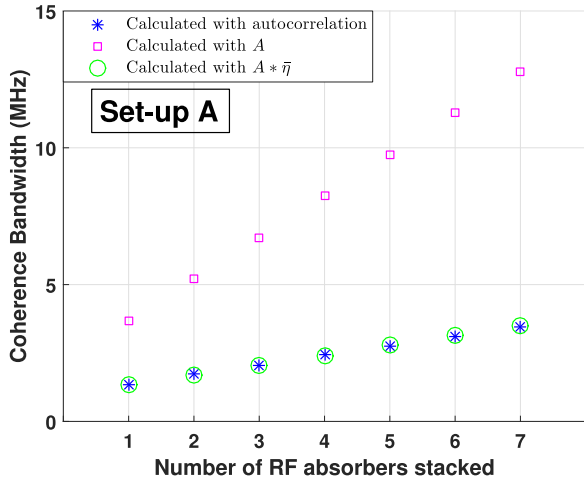
Fig. 7. CBW calculated for the PCS band from (8) (stars), CBW calculated from the exposed absorber surface area as ACS in (10) (squares), and CBW calculated from the exposed absorber surface area times $\bar{\eta}$ (0.23) from Fig. 6 as ACS in (10) (circles). CBWs are calculated for different loadings of the RC.

In Fig. 7, we see that the predicted and measured CBWs match well, implying that the CBW for a different loading case can be predicted if the ratio between the ACS and the exposed surface area of the new RF absorber is known, i.e., if the average absorber's efficiency $\bar{\eta}$ is known. Note that η can be experimentally determined or sometimes be obtained from the manufacturer's datasheets. It generally depends on used materials, shape, and placement in the RC. In this study we focus on η determined experimentally.

Table III gives the $\bar{\eta}$ calculated from (17) with $\langle \text{ACS} \rangle$ from (9) ($\bar{\eta}_{\text{CBW}}$), $\langle \text{ACS} \rangle$ from (5) ($\bar{\eta}_{\tau_{\text{RMS}}}$), and $\langle \text{ACS} \rangle$ from (15) ($\bar{\eta}_{G_{\text{ref}}}$) for all setups used. This table also includes the maximum difference Δ_{max} between the measured and predicted CBW, τ_{RMS}, and G_{ref} for all loading conditions with the prediction based on (10) (CBW), (6) (τ_{RMS}), or (16) (G_{ref}). Some values of $\bar{\eta}$ round to 0.25, which suggests ideal absorbers. In practice, the absorbers were not ideal, but uncertainties in the absorbers dimensions and RC measurements can cause $\bar{\eta}$ to round to 0.25.

In this section, we showed that measured ratio between the ACS and the lossy object's surface area (η) is nearly constant. Because η is nearly constant, a determination of η from any single loading condition is sufficient. Therefore, we can predict the total ACS by knowing the total surface area of all absorbers used inside the chamber and correction factor η determined from a single loading condition. In the next section, we will illustrate that this idea can save enormous amount of time when setting-up the chamber for various wireless measurements.

C. Predicting CBW, τ_{RMS}, and G_{ref} From a Single Loading Condition

For over-the-air (OTA) tests of wireless devices, measuring the S-parameters for all loading cases can be very time intensive and the procedure described here can reduce this time. The approach is based on well-known linear relationship between the ACS and surface area [21]. Assuming this linear model, we can predict the ACS by knowing η and the absorbers surface

TABLE IV
MAXIMUM DIFFERENCE BETWEEN MEASURED AND PREDICTED CBW, τ_{RMS}, AND G_{REF} PREDICTED FROM A SINGLE LOADING CONDITION

Setup	Δ_{max} CBW (%)	Δ_{max} τ_{RMS} (%)	Δ_{max} G_{ref} (%)
A Cell	3.5	5.7	3.2
A *PCS*	*2.0*	*5.6*	*2.5*
B Cell	3.5	5.8	–
B *PCS*	*5.0*	*5.2*	–
C Cell	4.8	4.5	–
C *PCS*	*3.1*	*3.5*	–
D *PCS*	*5.0*	*6.2*	–

TABLE V
PERCENT DIFFERENCE BETWEEN MEASURED AND PREDICTED CBW OBTAINED FROM (10) USING A SINGLE LOADING CASE FOR THE PREDICTION. SETUP A WAS USED: 1–7 STACKED ABSORBERS

Loading condition used to determine η	Predicted loading condition						
	1	2	3	4	5	6	7
	Cell *PCS*	Cell *PCS*	Cell *PCS*	Cell *PCS*	Cell *PCS*	Cell *PCS*	Cell *PCS*
1	0	3.0	2.8	3.5	2.5	2.5	2.1
	0	*1.8*	*0.80*	*1.0*	*0.35*	*0.36*	*0.34*
2	2.7	0	0.47	0.076	1.1	1.2	1.6
	1.5	*0*	*1.1*	*1.1*	*1.8*	*1.9*	*2.0*
3	2.3	0.44	0	0.57	0.61	0.65	1.1
	0.62	*1.0*	*0*	*0.17*	*0.55*	*0.57*	*0.61*
4	2.8	0.068	0.55	0	1.2	1.3	1.7
	0.74	*0.89*	*0.16*	*0*	*0.73*	*0.75*	*0.80*
5	1.9	0.95	0.56	1.2	0	0.025	0.45
	0.24	*1.5*	*0.49*	*0.69*	*0*	*0.0013*	*0.027*
6	1.9	0.97	0.58	1.2	0.024	0	0.42
	0.24	*1.5*	*0.49*	*0.69*	*0.0013*	*0*	*0.026*
7	1.6	1.3	0.95	1.6	0.43	0.41	0
	0.22	*1.5*	*0.51*	*0.71*	*0.025*	*0.025*	*0*

area. We can now study the predictability of our method when η is derived from a single loading case for various setups.

Tables V–VIII show the percent difference between the predicted value of the CBW and the CBW calculated from S-parameters from (8) for Setup A to Setup D, respectively. We predicted the CBW for all loading cases using η calculated from one loading case and using (10). η was determined from (17) using (9) to calculate $\langle \text{ACS} \rangle$. The rows in the tables indicate different loading conditions used to calculate η. The columns indicate the predicted loading conditions. For Setup A, the maximum difference between the measured and predicted CBW is below 3.5% for every loading case used for the calculation.

In Table IV, we give the comparison in terms of maximum difference Δ_{max} between predicted and measured metrics (CBW, τ_{RMS} and G_{ref}) for different measurement setups, when η is derived from a single loading case. The maximum observed difference between measured and predicted CBW was below 5%. On the other hand, maximum difference between measured and predicted τ_{RMS} was below 6.2%, while predicted G_{ref} was in consistence with measured one within 3.2%, which corresponds to an uncertainty of 0.14 dB. This uncertainty is sometimes smaller than the measured uncertainty due to lack of spatial uniformity [10].

TABLE VI
PERCENT DIFFERENCE BETWEEN MEASURED AND PREDICTED CBW OBTAINED FROM (10) USING A SINGLE LOADING CASE FOR THE PREDICTION. SETUP B WAS USED: 1–5 ABSORBERS STANDING ON THE SIDE

Loading condition used to determine η	Predicted loading condition				
	1	2	3	4	5
	Cell	Cell	Cell	Cell	Cell
	PCS	*PCS*	*PCS*	*PCS*	*PCS*
1	0	0.28	3.2	3.2	0.63
	0	*4.0*	*0.61*	*0.49*	*0.47*
2	0.23	0	3.5	3.5	0.95
	3.0	*0*	*3.6*	*4.9*	*5.0*
3	2.6	3.4	0	0.11	2.9
	0.44	*3.4*	*0*	*1.1*	*1.1*
4	2.5	3.3	0.11	0	2.8
	0.34	*4.4*	*1.1*	*0*	*0.039*
5	0.46	0.84	2.6	2.6	0
	0.31	*4.4*	*1.1*	*0.037*	*0*

TABLE VII
PERCENT DIFFERENCE BETWEEN MEASURED AND PREDICTED CBW OBTAINED FROM (10) USING A SINGLE LOADING CASE FOR THE PREDICTION. SETUP C WAS USED: 1–4 PYRAMIDAL SHAPE ABSORBERS PLACED ON THE FLOOR

Loading condition used to determine η	Predicted loading condition			
	1	2	3	4
	Cell	Cell	Cell	Cell
	PCS	*PCS*	*PCS*	*PCS*
1	0	0.23	4.6	1.8
	0	*1.6*	*1.5*	*0.46*
2	0.20	0	4.8	2.1
	1.3	*0*	*3.1*	*2.2*
3	3.9	4.8	0	3.0
	1.2	*3.0*	*0*	*1.1*
4	1.5	2.0	2.9	0
	0.34	*2.0*	*1.0*	*0*

TABLE VIII
PERCENT DIFFERENCE BETWEEN MEASURED AND PREDICTED CBW OBTAINED FROM (10) USING A SINGLE LOADING CASE FOR THE PREDICTION. SETUP D WAS USED: 1–5 STACKED ABSORBERS IN A SMALL RC CALCULATED FOR THE PCS BAND

Loading condition used to determine η	Predicted loading condition				
	1	2	3	4	5
1	*0*	*1.5*	*0.99*	*0.078*	*3.4*
2	*1.3*	*0*	*0.60*	*1.7*	*5.0*
3	*0.81*	*0.56*	*0*	*1.1*	*4.4*
4	*0.062*	*1.6*	*1.1*	*0*	*3.3*
5	*2.7*	*4.7*	*4.3*	*3.3*	*0*

The previous measurements were made with square absorber blocks. We also measured absorbers having a pyramidal shape (Setup C). Table VII shows that the maximum difference between the predicted and measured CBW stays below 4.8%.

To investigate if the CBW prediction also works for other RCs, we measured a stack of absorbers in the small RC (Setup D). The RCs used in these experiments are representative for determining CBW, τ_{RMS}, and G_{ref}. Tanuhardja *et al.* [9], [10], [18] used these RCs before to determine chamber characteristics. The resulting difference between the predicted and measured CBW based on a measurement of the unloaded RC and one loading case is shown in Table VIII for the PCS band. For this RC, the maximum difference between the predicted and measured CBW stays below 5.0%.

V. CONCLUSION

In this paper, we developed a method to predict the CBW, τ_{RMS}, and G_{ref} of a loaded RC based on a measurement of an unloaded RC and a measurement of a single loading case whose exposed surface area is known. Note that we restricted our study on RF absorber blocks as loading material. Common DUTs and real RC fixtures can also load the chamber and consequently change CBW, τ_{RMS}, and G_{ref}. However, this is beyond the scope of this study. We relate the ACS of a single loading case to the actual exposed surface area of the RF absorber to predict the ACS of other loading cases. The maximum difference between the predicted and measured CBW, τ_{RMS}, and G_{ref} stays below 6.2% for different types of absorbing materials, different shapes and placements of the absorber and different RCs.

We also looked at the frequency spacing of the VNA measurements that is needed for the calculation of the CBW, τ_{RMS}, and G_{ref}. For the setups we studied, a smaller frequency spacing is needed for the calculation of τ_{RMS} than for the calculation of CBW. For the calculation of G_{ref}, the frequency spacing is not strict. We also saw that RCs that provide a narrower CBW when unloaded (e.g., larger chambers) require a smaller frequency spacing than RCs with a wider unloaded CBW.

The method developed here can reduce the test time for OTA testing of cellular devices in RCs. In particular, this refers to tests such as TIS, where it is necessary to load the chamber to widen the CBW. To set up the RC, first measure *S*-parameters of an unloaded RC. Measure the RC loaded with RF absorbers with a known amount of exposed surface area after that. Finally,

To illustrate that the 5% difference in CBW is not significant compared to other factors, such as the choice of the autocorrelation threshold, we calculated the CBW for a single loading condition and setup with two different threshold values. For the calculation of the CBW from the autocorrelation, we used a threshold of 0.5. This threshold is not the only threshold that can be used. Values like 0.7 and $1/e$ can also be used as a threshold [18]. We calculated the percent difference of the CBW calculated with a threshold of 0.5 and 0.7 for Setup A with seven RF absorbers. The difference between the calculated CBWs with different threshold values is 42.5%. We conclude that the difference between the predicted and measured CBW (5.0%) is not significant, relative to the difference caused by a different threshold.

In Setup B, the absorbers are placed individually on their sides, resulting in a much heavier loading condition than the absorber stack used in Setup A because of the increased exposed surface area A. The difference between the prediction and measurement of the CBW for the cell and PCS bands can be found in Table VI. This table shows that for this setup, the maximum difference between the prediction and measurement of CBW is below 5.0%.

calculate the amount of absorbers needed to obtain the desired CBW, τ_{RMS} or G_{ref}.

Possible future work includes research on the restrictions of this method and on the range of the maximum difference between predicted and measured RC characteristics.

ACKNOWLEDGMENT

The authors would like to thank C. Weldon for help with the measurements and D. Ribeiro for help with the automation of the data acquisition.

REFERENCES

[1] C. L. Holloway, D. A. Hill, J. M. Ladbury, P. F. Wilson, G. Koepke, and J. Coder, "On the use of reverberation chambers to simulate a rician radio environment for the testing of wireless devices," *IEEE Trans. Antennas Propag.*, vol. 54, no. 11, pp. 3167–3177, Nov 2006.

[2] X. Chen and P.-S. Kildal, "Theoretical derivation and measurements of the relationship between coherence bandwidth and RMS delay spread in reverberation chamber," in *Proc. Eur. Conf. Antennas Propag.*, Mar. 2009, pp. 2687–2690.

[3] X. Chen, P.-S. Kildal, C. Orlenius, and J. Carlsson, "Channel sounding of loaded reverberation chamber for over-the-air testing of wireless devices—Coherence bandwidth versus average mode bandwidth and delay spread," *IEEE Antennas Wireless Propag. Lett.*, vol. 8, pp. 678–681, Jun. 2009.

[4] E. Genender, C. L. Holloway, K. A. Remley, J. M. Ladbury, G. Koepke, and H. Garbe, "Simulating the multipath channel with a reverberation chamber: Application to bit error rate measurements," *IEEE Trans. Electromagn. Compat.*, vol. 52, no. 4, pp. 766–777, Nov. 2010.

[5] K. A. Remley, S. J. Floris, H. A. Shah, and C. L. Holloway, "Static and dynamic propagation-channel impairments in reverberation chambers," *IEEE Trans. Electromagn. Compat.*, vol. 53, no. 3, pp. 589–599, Aug 2011.

[6] C. L. Holloway, H. A. Shah, R. J. Pirkl, K. A. Remley, D. A. Hill, and J. Ladbury, "Early time behaviour in reverberation chambers and its effect on the relationships between coherence bandwidth, chamber decay time, RMS delay spread, and the chamber buildup time," *IEEE Trans. Electromagn. Compat.*, vol. 54, no. 4, pp. 714–725, Aug 2012.

[7] P.-S. Kildal, X. Chen, C. Orlenius, M. Franzén, and C. S. L. Patané, "Characterization of reverberation chambers for OTA measurements of wireless devices: Physical formulations of channel matrix and new uncertainty formula," *IEEE Trans. Antennas Propag.*, vol. 60, no. 8, pp. 3875–3891, Aug 2012.

[8] S. van de Beek, K. A. Remley, C. L. Holloway, J. M. Ladbury, and F. Leferink, "Characterizing large-form-factor devices in a reverberation chamber," in *Proc. Int. Symp. Electromagn. Compat.*, Brugge, Belgium, Sept. 2013, pp. 375–380.

[9] R. R. Tanuhardja, L. A. Gonzalez, C.-M. Wang, W. F. Young, and K. A. Remley, "Using the amplitude variation of a reverberation chamber channel to predict the synchronization of a wireless digital communication test system," in *Proc. IEEE Int. Symp. Electromagn. Compat.*, Dresden, Germany, Aug 2015, pp. 171–176.

[10] J. aan den Toorn, K. A. Remley, C. L. Holloway, J. M. Ladbury, and C.-M. Wang, "Proximity-effect test for lossy wireless-device measurements in reverberation chambers," *IET Sci., Meas. Technol.*, vol. 9, no. 5, pp. 540–546, 2015.

[11] C. E. Shannon, "A mathematical theory of communication," *Bell Syst. Tech. J.*, vol. 27, no. 3, pp. 379–423, Jul. 1948.

[12] K. A. Remley, C.-M. Wang, D. F. Williams, J. aan den Toorn, and C. L. Holloway, "A significance test for reverberation chamber measurement uncertainty in total radiated power of wireless devices," *IEEE Trans. Electromagn. Compat.*, vol. 58, no. 1, pp. 207–219, Feb. 2016.

[13] M. I. Andries, P. Besnier, and C. Lemoine, "On the prediction of the average absorbing cross section of materials from coherence bandwidth measurements in reverberation chambers," in *Proc. Int. Symp. Electromagn. Compat.*, Rome, Italy, 2012, pp. 1–6.

[14] E. Amador, M. I. Andries, C. Lemoine, and P. Besnier, "Absorbing material characterization in a reverberation chamber," in *Proc. 10th Int. Symp. Electromagn. Compat.*, York, U.K., Sep. 2011, pp. 117–122.

[15] T. Nguyen, "RF loading effects of aircraft seats in an electromagnetic reverberating environment," presented at the *Digital Avionics Systems Conf.*, St Louis, MO, USA, vol. 2, Oct 1999.

[16] D. Senić, A. Šarolić, and Z. M. Jóskiewicz, "Preliminary results of human body average absorption cross section measurements in reverberation chamber," in *Proc. Int. Symp. Electromagn. Compat.*, Brugge, Belgium, Sep. 2013, pp. 887–890.

[17] D. Hill, *Electromagnetic Fields in Cavities*. Hoboken, NJ, USA: Wiley, 2009.

[18] K. A. Remley *et al.*, "Configuring and verifying reverberation chambers for testing cellular wireless devices," *IEEE Trans. Electromagn. Compat.*, vol. 58, no. 3, Jun. 2016.

[19] U. Carlberg, P.-S. Kildal, A. Wolfgang, O. Sotoudeh, and C. Orlenius, "Calculated and measured absorption cross sections of lossy objects in reverberation chamber," *IEEE Trans. Electromagn. Compat.*, vol. 46, no.2, pp. 146–154, May 2004.

[20] D. Senić, C. L. Holloway, J. M. Ladbury, G. H. Koepke, and A. Šarolić, "Absorption characteristics and SAR of a lossy sphere inside a reverberation chamber," in *Proc. Int. Symp. Electromagn. Compat.*, Gothenburg, Sweden, Sep. 2014, pp. 962–967.

[21] I. D. Flintoft, M. P. Robinson, G. C. R. Melia, J. F. Dawson, and A. C. Marvin, "Average absorbtion cross-section of the human body measured at 1–12 GHz in a reverberant environment: Results of a human volunteer study," *Phys. Med. Biol.*, vol. 59, no. 13, pp. 3297–3317, Jul. 2014.

[22] A. Gifuni, "On the measurement of the absorption cross section and material reflectivity in a reverberation chamber," *IEEE Trans. Electromagn. Compat.*, vol. 51, no. 4, pp. 1047–1050, Nov. 2009.

[23] P. Hallbjörner, U. Carlberg, K. Madsén, and J. Andersson, "Extracting electrical material parameters of electrically large dielectric objects from reverberation chamber measurements of absorption cross section," *IEEE Trans. Electromagn. Compat.*, vol. 47, no. 2, pp. 291–303, May 2005.

[24] J. B. Coder, J. M. Ladbury, C. L. Holloway, and K. A. Remley, "Examining the true effectiveness of loading a reverberation chamber: How to get your chamber consistently loaded," in *Proc. IEEE Int. Symp. Electromagn. Compat.*, Fort Lauderdale, FL, USA, 2010, pp. 530–535.

Jos N. H. Dortmans was born in Helmond, The Netherlands. He received the B.Sc. degree in electrical engineering from the Eindhoven University of Technology, Eindhoven, The Netherlands, in 2015, where he is currently working toward the M.Sc. degree in electrical engineering.

In 2015, he was a Guest Researcher with the Electromagnetics Division, National Institute of Standards and Technology, Boulder, CO, USA. His current research interests include wireless communications and high-frequency measurements.

Kate A. Remley (S'92–M'99–SM'06–F'13) was born in Ann Arbor, MI, USA. She received the Ph.D. degree in Electrical and Computer Engineering from Oregon State University, Corvallis, OR, USA, in 1999.

From 1983 to 1992, she was a Broadcast Engineer with Eugene, OR, USA, serving as the Chief Engineer of an AM/FM broadcast station from 1989 to 1991. In 1999, she joined the RF Technology Division, National Institute of Standards and Technology (NIST), Boulder, CO, USA, as an Electronics Engineer. She is currently the Leader of the Metrology for Wireless Systems Group, NIST, where her research activities include development of calibrated measurements for microwave and millimeter-wave wireless systems, characterizing the link between nonlinear circuits and system performance, and developing standardized test methods for RF equipment used by the public-safety community.

Dr. Remley received the Department of Commerce Bronze and Silver Medals, the ARFTG Best Paper Award, and is a Member of the Oregon State University Academy of Distinguished Engineers. She was the Chair of the MTT-11 Technical Committee on Microwave Measurements from 2008 to 2010 and the Editor-in-Chief of IEEE MICROWAVE MAGAZINE from 2009 to 2011, and is the Chair of the MTT Fellow Committee. She is a Distinguished Lecturer for the IEEE Electromagnetic Compatibility Society (2016–2018).

Damir Senić (S'09–M'16) received the M.Sc. degree in 2008 and the Ph.D. degree in 2014, both from University of Split, Faculty of Electrical Engineering, Mechanical Engineering and Naval Architecture, Split, Croatia.

He is currently working at the University of Colorado Boulder working at National Institute of Standards and Technology, Communications Technology Laboratory in Boulder as a Postdoctoral Research Associate through Professional Research Experience Program. His research interests include millimeter wave radiocommunications, electromagnetic measurements, electromagnetic compatibility, and bioeffects of EM fields.

Dr. Senić received Richard E. Merwin Award of IEEE Computer Society for exemplary involvement in IEEE activities and excellent academic achievement in 2013.

Chih-Ming Wang received the Ph.D. degree in statistics from Colorado State University, Fort Collins, CO, USA, in 1978.

Since 1988, he has been with the Statistical Engineering Division, National Institute of Standards and Technology, Boulder, CO, USA. He has published more than 90 journal articles. His research interests include statistical metrology and the application of statistical methods to physical sciences.

Dr. Wang is a Fellow of the American Statistical Association (ASA). He received the Department of Commerce Silver Medal, Bronze Medal, the NIST Allen V. Astin Measurement Science Award, and several awards from ASA.

Christopher L. Holloway (S'86–M'92–SM'04–F'10) received the B.S. degree from the University of Tennessee at Chattanooga, Chattanooga, TN, USA, in 1986, and the M.S. and Ph.D. degrees from the University of Colorado Boulder, Boulder, CO, USA, in 1988 and 1992, respectively, both in electrical engineering.

In 1992, he was a Research Scientist with Electro Magnetic Applications, Inc., Lakewood, CO, USA. His responsibilities included theoretical analysis and finite-difference time-domain modeling of various electromagnetic problems. From the fall of 1992 to 1994, he was with the National Center for Atmospheric Research (NCAR) in Boulder, CO, USA. While at NCAR his duties included wave propagation modeling, signal processing studies, and radar systems design. From 1994 to 2000, he was with the Institute for Telecommunication Sciences, U.S. Department of Commerce, Boulder, CO, USA, where he was involved in wave propagation studies. Since 2000, he has been with the National Institute of Standards and Technology (NIST), Boulder, CO, USA, where he works on electromagnetic theory. He is also with the Graduate Faculty at the University of Colorado Boulder. His research interests include electromagnetic field theory, wave propagation, guided wave structures, remote sensing, numerical methods, metamaterials, measurement techniques, EMC/EMI issues, and atom-based metrology.

Dr. Holloway is a Member of URSI Commissions A, B, and E. He is currently serving as Chair for US Commission A of the International Union of Radio Science and is an Associate Editor for the IEEE TRANSACTIONS ON ELECTROMAGNETIC COMPATIBILITY. He was the Chairman for the Technical Committee on Computational Electromagnetics (TC-9) of the IEEE Electromagnetic Compatibility Society from 2000 to 2005, served as the Co-Chair for the Technical Committee on Nano-Technology and Advanced Materials (TC-11) of the IEEE EMC Society from 2006 to 2011, and served as an IEEE Distinguished Lecturer for the EMC Society from 2004 to 2006.